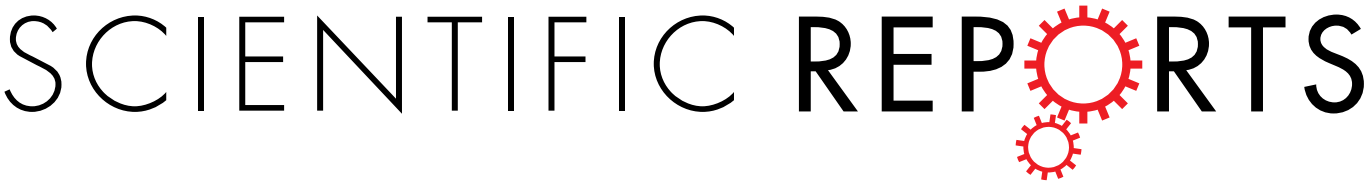

OPEN

Received: 22 September 2015
Accepted: 23 December 2015
Published: 04 February 2016

Hybrid coordination-network-engineering for bridging cascaded channels to activate long persistent phosphorescence in the second biological window

Xixi Qin[1,*], Yang Li[1,2,*], Ruili Zhang[3], Jinjun Ren[3], Mindaugas Gecevicius[1], Yiling Wu[1], Kaniyarakkal Sharafudeen[4], Guoping Dong[1], Shifeng Zhou[1], Zhijun Ma[1] & Jianrong Qiu[1]

We present a novel "Top-down" strategy to design the long phosphorescent phosphors in the second biological transparency window via energy transfer. Inherence in this approach to material design involves an ingenious engineering for hybridizing the coordination networks of hosts, tailoring the topochemical configuration of dopants, and bridging a cascaded tunnel for transferring the persistent energy from traps, to sensitizers and then to acceptors. Another significance of this endeavour is to highlight a rational scheme for functionally important hosts and dopants, Cr/Nd co-doped $Zn_{1-x}Ca_xGa_2O_4$ solid solutions. Such solid-solution is employed as an optimized host to take advantage of its characteristic trap site level to establish an electron reservoir and network parameters for the precipitation of activators Nd^{3+} and Cr^{3+}. The results reveal that the strategy employed here has the great potential, as well as opens new opportunities for future new-wavelength, NIR phosphorescent phosphors fabrication with many potential multifunctional bio-imaging applications.

There is an increasing interest in the use of long persistent phosphorescence in the biologically transparent window to drive the photonic bioprobe for tracing the cancer cells[1]. Long phosphorescent phosphors (LPPs) can help avoiding the challenging requirement of high-intensity illumination during the signal collection, which often leads to decreased signal-to-noise ratio and photon-induced deterioration of analytes[2]. This emerging research trend, which incorporates various fields of materials science, biology, chemistry, engineering, physics and pharmaceuticals, follows two main directions: operation waveband and persistent duration, with many relevant crossing points in between[3,4]. As we know, there are two biologically transparent windows: first one at 650–950 nm and second one at 1000–1350 nm[5]; Near-infrared (NIR) light in the first transparency window can penetrate biological tissues such as skin and blood more efficiently than visible light[6], yet the second region has even lower absorption and scattering therefore offers more efficient tissue penetration[7]. However, the main researches about the operational waveband of NIR LPPs mainly focus on the short wavelength region, i.e. first NIR window.

In addition to altering the emission center and tailoring the crystal field surrounding the activator, another useful strategy to extend the operational waveband, is to transfer the persistent energy of sensitizers to acceptors[8]. In fact, although the afterglow properties are predominantly controlled by the active traps, more subtle effects, such as topochemical coordination-configuration of dopant ions, can also have a profound role to the spectroscopic features of LPPs, which has long been recognized as a significant issue lying at the heart of doping chemistry and photoluminescent theory[9]. Considering the advanced engineering of cascaded tunnel of energy transfer

[1]State Key Laboratory of Luminescent Materials and Devices, Guangdong Provincial Key Laboratory of Fiber Laser Materials and Applied Techniques, South China University of Technology, Guangzhou 510640, China. [2]School of Chemistry and Chemical Engineering, South China University of Technology, Guangzhou 510640, China. [3]Shanghai institute of optics and fine mechanics, Chinese Academy of Sciences 201800, China. [4]Escola de Engenharia de Sao Carlos, Universidade de Sao Paulo, 13566-590, Sao Carlos, SP, Brazil. *These authors contributed equally to this work. Correspondence and requests for materials should be addressed to Y.L. (email: msliyang@scut.edu.cn) or J.Q. (email: qjr@scut.edu.cn)

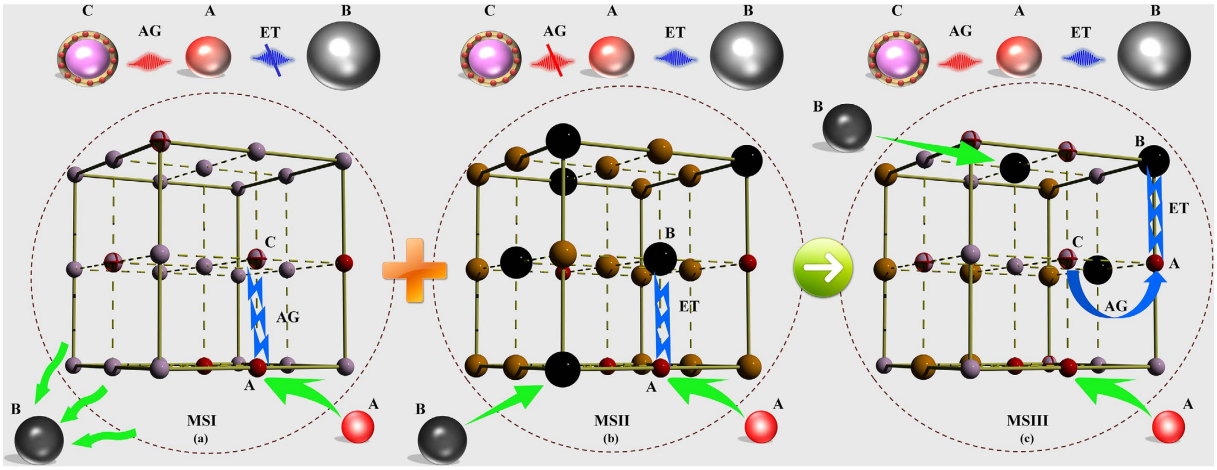

Figure 1. Schematic illustration showing the influence of ions doping-pattern and network-structural motifs on energy transfer process between traps and dopants. (**a,b**) represent the typical trapping and de-trapping process (AG) (traps (C) → activator (A)), as well as energy transfer process (ET) (activator (A) → activator (B)) in different material system (MSI and MSII), respectively. Hybrid Materials (MSIII) involves a solid-solution to offer the suitable coordination geometry for activators (A) and (B), and realize the cascaded energy transfer (traps (C) → activator (A) → activator (B)).

(traps → activator(A) → activator(B)) and going into the details of it, one has at one's disposal several decades worth of well-established principles in the coincident matching of macroscopical and microscopic features in spectroscopy, coordination chemistry and network connectivity relating to activators and hosts[10,11]. Traditionally, materials scientists view such network-engineering design accessed via active impurities with a practical eye intent on describing integral architectures in terms of ion types, valency and radius, local coordination geometries, as well as their concomitant implications for electronegativity and chemical bonding[12]. However, due to the complex attribute of topological network, there are still remaining grand challenges: to gain better modulation for the local coordination configuration of dopants, to understand the principle linking the indispensable transfer channel of independent individual, and to realize true predictability to the arrangements of traps and dopants (sensitizers, activators, or co-dopants) in coordinated network.

In this work we present a new "Top-down" approach to design and synthesize the long phosphorescent phosphors in the second biological transparent window. The material design approach employed here involves an ingenious engineering for hybridizing the coordination networks of hosts, tailoring the topochemical configuration of dopants, and bridging cascaded channels for transferring the persistent energy from traps, to sensitizers, to acceptors. We present a closed energy transfer channel from Cr^{3+} to Nd^{3+} in $ZnGa_2O_4$ phosphor and invalid electronic reservoir in $CaGa_2O_4$ phosphor, respectively. Persistent energy-transfer could occur in $Zn_{1-x}Ca_xGa_2O_4$ solid-solution because two dopants were successfully locked in a cage via the efficient crystal packing at an appropriate distance, in addition to the preservation of native electron traps. The hybrid network topologies and structural motifs, thus far will be outlined with particular emphasis on how specific route of energy transfer can be prepared via premeditatedly designing a material system. Such design strategy will notably open a vista of potential avenues for the design of new optical functional materials for the future.

Results and Discussion

Our strategy was inspired by the fundamental spectroscopic theory of energy transfer and local intercalation reaction in inorganic polycrystals (Fig. 1)[13]. In our view, a typical long phosphorescent phosphor (MSI, in Fig. 1a) features a prominent electron reservoir (C, in Fig. 1) with the distinct ability of storing and releasing the captured electrons, as well as a notable photon-emitter (A, in Fig. 1) with higher quantum efficiency under the condition of accurately matching lattice-coordination network and atomic radius[14]. A pre-established electronic transfer channel (AG, traps (C) → activator (A), in Fig. 1) ensures the long persistent phosphorescence. However, the topological network does not provide an opportunity for another activator (B, in Fig. 1) to embed itself into the suitable lattice site. Such structural constraint thus, closes the possible channel of energy transfer (ET, in Fig. 1) between (A) and (B), leading to the luminescent and phosphorescent quenching. Fortunately, the existing chemical and spectroscopic knowledge offer a far-sighted technique to select another material system (MSII, in Fig. 1b), which allows a synchronous precipitation of activator (A) and (B), as well as engineers a theoretically existent energy-transfer channel (activator (A) → activator (B)). But to our surprise, this scheme misses the necessary electron reservoir so as to completely decrease the probability of electrons trapping-detrapping (Fig. 1b).

The use of solid-solution complexes to engineer predictable, multi-dimensional infinite networks has received ever-increasing attention in the area of chemistry and materials science[15]. Solid-solutions have already proven their superiorities in the areas of optical, optoelectronic, electrical and magnetic properties than the single component[16]. Pan *et al.* broke new ground in the field by using zinc gallogermanates solid-solution as the system, thereby achieving a super-long NIR afterglow emission time of 360 h[3]. Kobayashi *et al.* also demonstrated

a state-of-the-art Li_xFePO_4 solid-solution technology, opening the door for lithium ion batteries to take their place in large-scale applications[17]. In addition, a series of solid-solution, such as $AgGa_{1-x}Al_xO_2$, $Zn_{1-x}Cu_xS$, $(SrTiO_3)_{1-x}(LaTiO_2N)_x$, also have been developed and used as the advanced photocatalysts to enhance the photocatalytic activity of a given semiconductor photocatalyst[18]. Therefore, solid-solution highlights hybrid coordination network of host, and is expected to open up a possibility in the visualization of the structural and functional binding process of traps and all activators into an independent system[19]. By rationally deploying an indirect intercalation complex comprised by polyhedron ligands of materials (MSI) and (MSII), hybrid coordination-network of novel solid-solution (MSIII, in Fig. 1c) is engineered to steady the activators (A) and (B), modulate the topochemical configuration of activators, and realize the cascaded energy transfers, traps(C) → activator(A) → activator(B) (Fig. 1c). Such novel structural motif is anticipated to adopt a disturbance to native unit cell and bridging a predictable periodic coordination network.

To validate research idea, a typical NIR long phosphorescent phosphor $ZnGa_2O_4$: Cr was pursued as preferential material system, which has been proven capable of supporting high defect densities, thought to be associated primarily with Zn vacancies (V_{Zn}) and O vacancies (V_O), as well as some antisite deficiencies (Zn_{Ga})[20]. Making use of its defect capacity, $ZnGa_2O_4$: Cr has been demonstrated as a NIR photo-emitter with surprisingly long persistent phosphorescence in first NIR window (Supplementary Fig. S1). Here, we target the operating waveband in the second NIR window by transferring the persistent energy of Cr^{3+} to Nd^{3+} in Cr/Nd-codoped $ZnGa_2O_4$ LPPs. Nd^{3+} ion is chosen as the emission center in order to take advantage of the appropriate energy level characteristic, i.e. NIR-absorption (680, 750 and 800 nm) and NIR emission (1064 nm)[21]. The various sharp transitions of Nd^{3+} [$^4I_{9/2} \rightarrow {}^4F_{5/2}$], [$^4I_{9/2} \rightarrow {}^4F_{7/2}$], [$^4I_{9/2} \rightarrow {}^4F_{9/2}$], just overlap the electron transition from metastable state ($^4T_2$) to ground state ($^4A_2$) of Cr^{3+}, allowing the potential energy transfer from Cr to Nd[22]. However, no any NIR phosphorescence in the second NIR window can be observed in Cr/Nd-codoped $ZnGa_2O_4$ LPPs (Fig. 2a). In fact, the desired phosphorescence is still absent in Nd^{3+} singly doped $ZnGa_2O_4$ phosphor after ceasing the excitation (Supplementary Fig. S2). It is notable that the diffuse reflection spectrum consists of the characteristic transition bands centered at 530, 588, 688, 748 and 808 nm, respectively, corresponding to Nd^{3+} f-f transition, [$^4I_{9/2} \rightarrow {}^2K_{13/2} + {}^4G_{7/2} + {}^4G_{9/2}$], [$^4I_{9/2} \rightarrow {}^2G_{7/2} + {}^2G_{5/2}$], [$^4I_{9/2} \rightarrow {}^4F_{9/2}$], [$^4I_{9/2} \rightarrow {}^4F_{7/2}$], [$^4I_{9/2} \rightarrow {}^4F_{5/2}$] in Nd^{3+} doped $ZnGa_2O_4$ phosphor (Supplementary Fig. S3)[21]; yet under the excitation at 748 nm, emission peak at 1064 nm, attributed to Nd^{3+} [$^4F_{3/2} \rightarrow {}^4I_{11/2}$] transition is not identifiable (Supplementary Fig. S4). This attractive optical quenching-phenomenon of luminescence and phosphorescence may be not concerned with the trap distribution, but the microcosmic network architecture.

In $ZnGa_2O_4$, a majority of [Ga^{VI}] cations occupy octahedral sites, whereas all of the [Zn^{IV}] cations occupy tetrahedral sites[23]. As a preliminary conjecture, Cr^{3+} has proven its strong ability to substitute for Ga^{3+} in distorted octahedral coordination, whereas Nd^{3+} cannot be effectively introduced into this specific network configuration (inset of Fig. 2a). In order to identify this possibility of ion doping, we focus on the intricate topochemical coordination geometry of Cr and Nd ions in zinc gallate spinel. The elucidation is performed in detail by a combination of XRD data and ^{71}Ga solid state nuclear magnetic resonance (NMR) studies. XRD patterns of $ZnGa_2O_4$: xCr (x = 0.5%, 5%, 10% and 20%) and $ZnGa_2O_4$: xNd (x = 0.5%, 5%, 10% and 20%) phosphors were measured and shown in Fig. 2b, Supplementary Fig. S5, S6. The peaks in XRD patterns of all Cr-doped samples are well indexed to pure $ZnGa_2O_4$ spinel structure (JCPDS 86-0848). In stark contrast, the higher doping content (up to 5%) of Nd ion gives rise to an impure phase, $NdGaO_3$ (JCPDS, 70-3810) in Nd-doped samples. Another interesting phenomenon, i.e. XRD dominated peak (PI in Fig. 2b) shifting towards to higher 2θ value with the increment of Cr content, reveals a small linear variation in $ZnGa_2O_4$ unit cell lattice parameter with Cr^{3+} substitution, whereas no any shift of same peak is observed in Nd-doped samples, further ensuring the distinct phase splitting (Fig. 2c). In addition, a decline of the peak intensity in Fig. 2c also is present. Nevertheless, the causes of this decline may be different and rooted from either the substitution or the phase splitting.

NMR allows the observation of specific quantum mechanical and magnetic properties of atomic nucleus, as well as provides the detailed information about the structure, dynamics, reaction state, and chemical environment of molecules[24]. Many scientific techniques exploit NMR phenomena to cover the interplay between the ligands and geometric centers, as well as study the topological network motif in crystals, microcrystalline powders, or anisotropic solutions, etc[25]. ^{71}Ga solid-state NMR is famous for the permission of quantitative analyses to different Ga^{3+} central coordination state in inorganic solids[26]. Figure 2d,e shows the systematical physical investigations of Ga coordination geometry in Cr and Nd singly doped $ZnGa_2O_4$, respectively. For the undoped $ZnGa_2O_4$ samples, ^{71}Ga NMR spectra exhibit two well-resolved resonances. The relative higher intensive signal at about 31 ppm is characteristic of sixfold coordinated Ga atoms, and the other weaker one ~at 170 ppm corresponds to Ga atoms in the tetrahedral sites of the spinel structure[26]. It is necessary to mention that with increasing Cr content (from 0.5% to 10%), ^{71}Ga NMR spectra present a significant broadening of spectral lines (Fig. 2d). In prominent contrast, scarcely any distinct influence on NMR spectral lines can be found by varying the Nd doping content in solid NMR spectra of $ZnGa_2O_4$: xNd (x = 0.5% and 10%) phosphors (Fig. 2e). The clear separation of NMR chemical shift at ~31 ppm between the two samples implies the precipitation of Cr^{3+} into the octahedral lattice site and the excludability of local configuration to Nd^{3+} ions. The NMR results are in accordance with XRD data, offering a powerful structural evidence to explain the interesting phenomena of phase splitting and luminescence quenching.

Actually, rare-earth elements generally form complexes which have high coordination numbers (CNs) and weak metal-ligand bonds, because of their large ionic radii and relatively low oxidation states[27]. Typically transition-metal and main-group elements have coordination numbers 2–6, while rare-earth metals have CNs > 6[28]. The resulting coordination polyhedra include trigonal prisms (CN = 6) or its variation by stepwise capping of the prism face up to CN = 9, in addition to square antiprisms (CN = 8); Coordination number 3 is realized only under extreme conditions[28]. Therefore, to supply an ideal dwelling for Nd^{3+}, a suitable material system should be proposed. Alkaline-earth metals have large ionic radii and various coordination-numbers 3–8

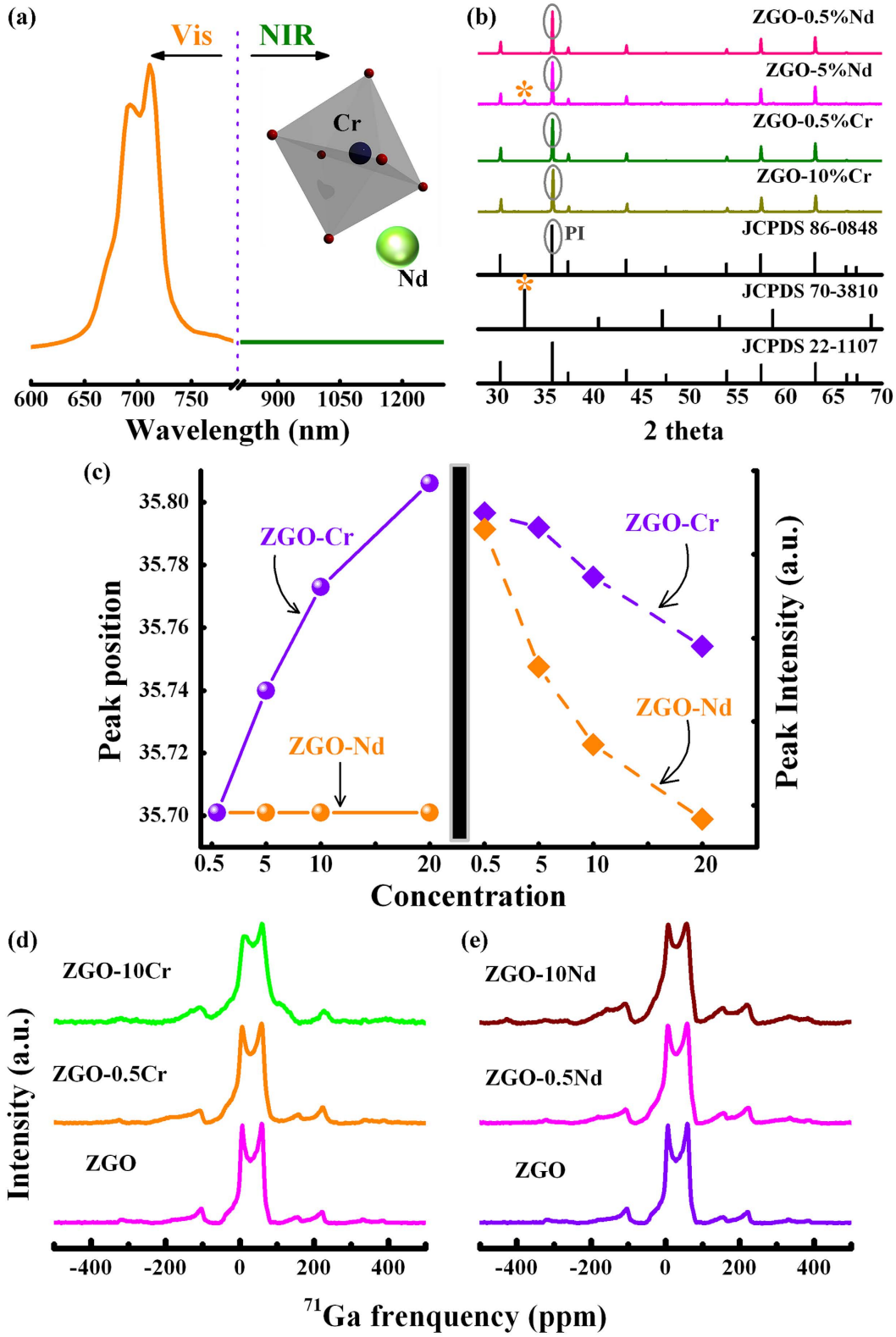

Figure 2. (**a**) Vis-NIR long persistent phosphorescence spectrum of $ZnGa_2O_4$: Cr/Nd phosphor. The inset shows a conjectural doping pattern of Cr and Nd. (**b**) XRD patterns for $ZnGa_2O_4$: xCr (x = 0.5% and 10%) and $ZnGa_2O_4$: xNd (x = 0.5% and 5%) phosphors. (**c**) Dependence of XRD peak ([PI] labeled in Fig. 2b) position and intensity as a function of Cr and Nd concentration in $ZnGa_2O_4$ phosphor. (**d–e**) ^{71}Ga solid state NMR spectra of $ZnGa_2O_4$: xCr (x = 0.5% and 10%) and $ZnGa_2O_4$: xNd (x = 0.5% and 10%) samples. All spectra were recorded at a magnetic field of 11.7 T with a sample spinning frequency of 25 kHz.

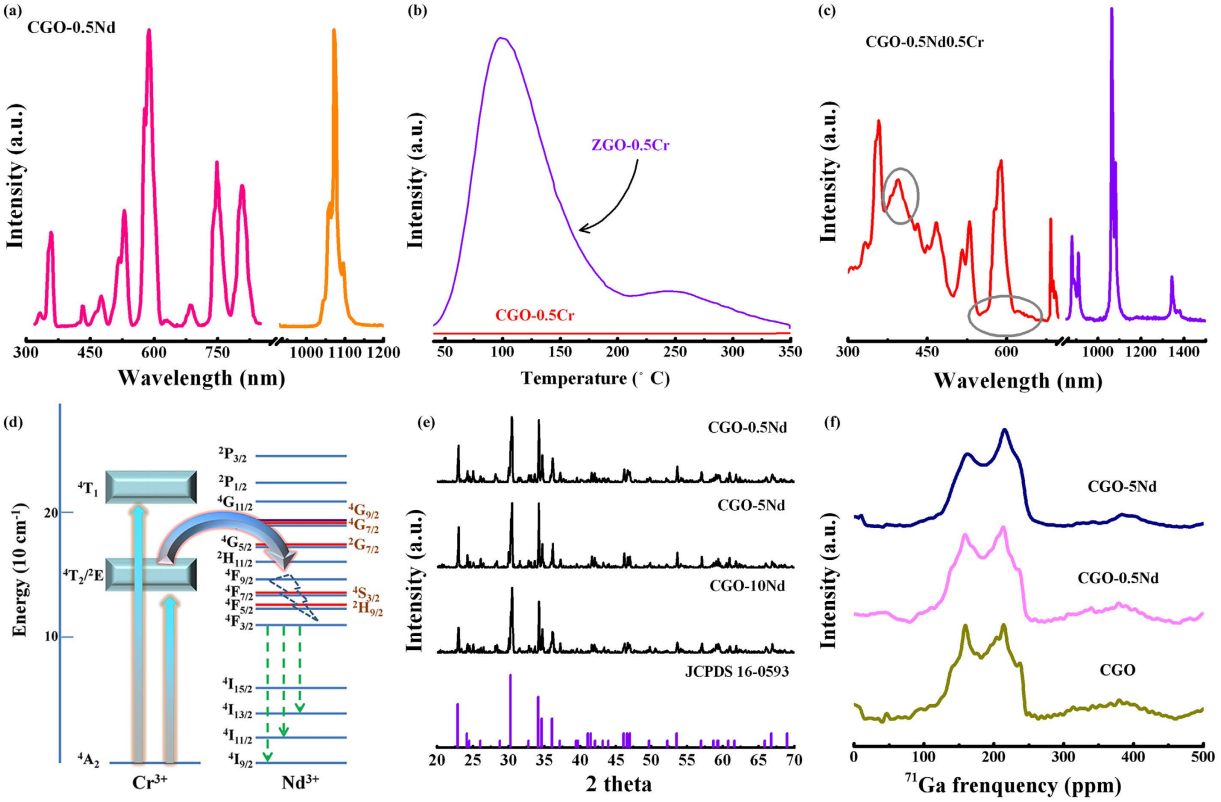

Figure 3. (**a**) Static photoluminescence spectrum under excitation at 750 nm and the corresponding photoluminescence excitation spectrum monitored at 1064 nm of CGO-0.5Nd phosphor; (**b**) Thermoluminescence curves of 0.5%Cr-doped $ZnGa_2O_4$ and $CaGa_2O_4$ phosphors measured 30 s after irradiation ceased; (**c**) Photoluminescence spectrum under excitation at 410 nm and photoluminescence excitation spectrum monitored at 1064 nm of CGO-0.5Cr0.5Nd phosphor; (**d**) Schematic illustration showing the energy-level diagram of Cr^{3+} and Nd^{3+} in $CaGa_2O_4$ phosphors; (**e**) XRD patterns for $CaGa_2O_4$: xNd (x = 0.5%, 5% and 10%) phosphors; (**f**) ^{71}Ga NMR spectra of $CaGa_2O_4$: xNd (x = 0, 0.5% and 5%) samples.

in different hosts, which ensure the selection of alkaline-earth gallates[29]. $CaGa_2O_4$ has a similar spinel crystal structure with $ZnGa_2O_4$. In $CaGa_2O_4$, [Ca^{VI}] cations occupy octahedral sites[29]. This configuration thus features a path of easy doping ion precipitation into the octahedral [Ca^{VI}] under the condition of matching geometrical lattice and atomic radius, which occurs with rare earth ion, Nd.

As expected, Fig. 3a exhibits the characteristic transitions of Nd^{3+} in Nd singly doped $CaGa_2O_4$ phosphor. However, the idealistic and aspirational long persistent phosphorescence is still absence in Cr singly, Nd singly and Cr/Nd doped $CaGa_2O_4$ phosphors, respectively (Supplementary Fig. S7). A possible cause of this problem is due to the lack of effective traps (Fig. 3b). In sharp contrast to Cr/Nd codoping $ZnGa_2O_4$, photoluminescence excitation (PLE) spectrum monitored at 1064 nm of Cr/Nd codoping $CaGa_2O_4$ sample consists of two specific excitation bands centered at ~410 and ~620 nm, in addition to Nd^{3+} characteristic f-f transitions (Fig. 3c), indicating an energy transfer from Cr^{3+} to Nd^{3+}. Obviously, the strong one is attributed to the Cr^{3+} [$^4A_2 \rightarrow {}^4T_1$], while the weak one corresponds to Cr^{3+} [$^4A_2 \rightarrow {}^4T_2$][30]. Further verification of energy transfer between Cr^{3+} and Nd^{3+} is supplied by emission spectrum and decay curve monitored at 1064 nm under the excitation wavelength at 410 nm (Fig. 3c and Supplementary Fig. S8). A possible channel of energy transfer from Cr^{3+} to Nd^{3+} is Cr^{3+} [$^4T_2 \rightarrow {}^4A_2$]: Nd^{3+} [$^4I_{9/2} \rightarrow {}^4F_{5/2}$], [$^4I_{9/2} \rightarrow {}^4F_{7/2}$], or [$^4I_{9/2} \rightarrow {}^4F_{9/2}$], depending on the overlap between Cr^{3+} emission band and Nd^{3+} absorption band (Fig. 3d)[31]. As discussed above, due to the similar atomic radius and geometric configurations, Nd ions can easily precipitate on Ca lattice site in $CaGa_2O_4$, enabling the distinct photoluminescence (PL). To probe the lattice configuration and substitution progress in $CaGa_2O_4$, we performed XRD and solid state NMR experiments. X-ray diffraction pattern first confirms the crystallization of Nd-doped calcium gallate (Fig. 3e). In contrast to Nd-doped $ZnGa_2O_4$, all Nd-doped $CaGa_2O_4$ samples can be indexed as standard phase $CaGa_2O_4$ (JCPDS 16-0593). There is no any apparent observation of phase splitting from XRD data, even under a higher doping content of Nd^{3+}, firmly supporting the rational inclusion of Nd^{3+} into an inert matrix, $CaGa_2O_4$. This result is also supported by ^{71}Ga solid state NMR spectra. In contrast to $ZnGa_2O_4$ host, the undoped $CaGa_2O_4$ sample has a dominant chemical shift at 170 ppm (Fig. 3f). With increasing dopants content, $CaGa_2O_4$: Nd also has the same effect of NMR resonances' line broadening and the linear increase of NMR resonances integrated intensity, strongly suggesting the successful substitution in substantial amounts of Nd into Ca lattice site.

Seemingly, as the individual backbone, MGa_2O_4 (Zn and Ca) polymorph is chosen as the prototypical coordination network for its respective ability to engineer the functionally independent tunnel, traps(C) →

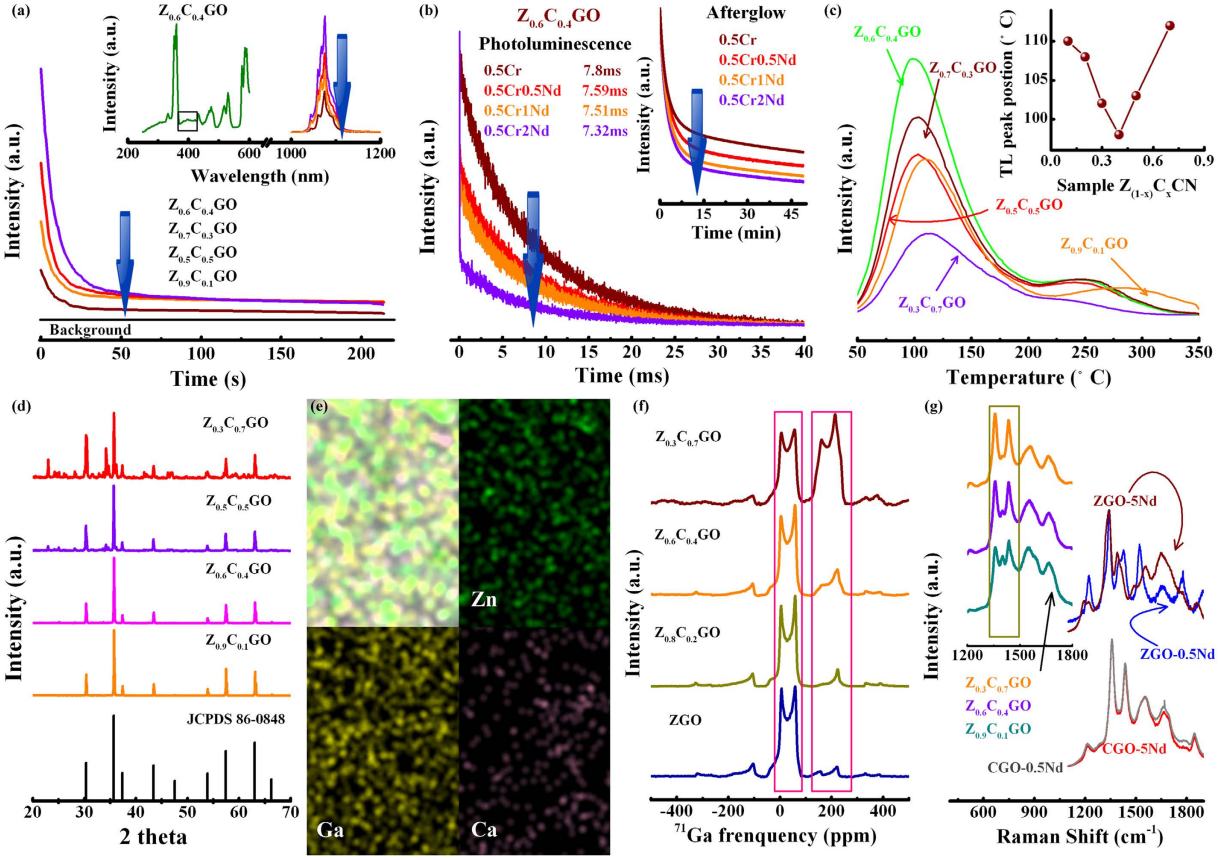

Figure 4. (**a**) persistence time monitored at 1064 nm as a function of Ca concentration (x = 0.1, 0.3, 0.4 and 0.5). The inset shows the long persistent phosphorescence spectra of $Z_{1-x}C_xGO$ (x = 0.1, 0.3, 0.4 and 0.5) samples and photoluminescence excitation spectrum monitored at 1064 nm of sample $Z_{0.6}C_{0.4}GO$. (**b**) Normalized photoluminescent and phosphorescent decay curves of $Z_{0.6}C_{0.4}GO$: 0.5%Cr/xNd (x = 0, 0.5%, 1% and 2%) samples. The monitored transition is Cr^{3+} [$^4T_2 \rightarrow {}^4A_2$]. (**c**) Thermoluminescence curves of $Z_{1-x}C_xGO$ (x = 0.1, 0.3, 0.4, 0.5 and 0.7) phosphors measured 30 s after irradiation ceased. The inset shows the dependence of TL peak position as a function of Ca concentration. (**d**) XRD patterns for $Z_{1-x}C_xGO$ (x = 0.1, 0.4, 0.5 and 0.7) phosphors. (**e**) EDX mapping of sample $Z_{0.6}C_{0.4}GO$. (**f**) ^{71}Ga NMR spectra of $Z_{1-x}C_xGO$ (x = 0, 0.2, 0.4 and 0.7) phosphors. (**g**) Normalized Raman spectra of ZGO-0.5Nd, ZGO-5Nd, CGO-0.5Nd, CGO-5Nd and $Z_{1-x}C_xGO$ (x = 0.1, 0.4 and 0.7) phosphors.

activator(A), or activator(A) → activator(B), used to transfer the required energy. The only regret is the fundamentally missing connection of traps(C) → activator(A) → activator(B) in a separate material system. To address this issue, we anticipate a novel solid-solution $Zn_{1-x}Ca_xGa_2O_4$ to bridge a new channel for transferring the persistent energy from traps to desired ions, based on the cautious consideration for crystal structure, ion valency and chemical bond relating to hosts and dopants. The desired NIR phosphorescence at 1064 nm is finally present in the afterglow spectra of $Zn_{1-x}Ca_xGa_2O_4$ (x = 0.1, 0.3, 0.4 and 0.5) solid-solution (Fig. 4a). Significantly, we also observe a strong dependence (i.e. rising first followed by a decline) of phosphorescent peak intensity and decay dynamics on Ca concentration in Fig. 4a. We attribute this special spectral change of Nd^{3+} to the successful persistent energy transfer from Cr^{3+} to Nd^{3+}, which is supported by the meticulous spectral studies of Nd^{3+} in an optimal $Zn_{0.6}Ca_{0.4}Ga_2O_4$: 0.5Cr/0.5Nd solid-solution: PLE band at 410 nm should be assigned to Cr^{3+} transition [$^4A_2 - {}^4T_2$], while a distinct NIR PL peak at 1064 nm is observed under the excitation at 410 and 600 nm (Fig. 4a and Supplementary Fig. S9). The additional support for the formation of an unrestricted energy tunnel, traps → Cr^{3+} → Nd^{3+}, is the analysis of kinetic processes in $Z_{0.6}C_{0.4}GO$: 0.5%Cr/xNd (x = 0, 0.5%, 1% and 2%) samples (Fig. 4b). PL decay dynamics study of Cr^{3+} shows a notable shortening in decay lifetime from 7.8 ($Z_{0.6}C_{0.4}GO-0.5Cr$), to 7.59 ($Z_{0.6}C_{0.4}GO-0.5Cr0.5Nd$), to 7.32 ms ($Z_{0.6}C_{0.4}GO-0.5Cr2Nd$), giving clear evidence of successfully simultaneous precipitation of two activators into the corresponding lattice along with the effective energy transfer from Cr^{3+} to Nd^{3+}.

It should be noted that, to the best of our knowledge, this type of NIR long-persistence phosphorescence has not been previously reported to occur in hybrid coordination networks by engineering cascaded energy transfer channels. Such substantial progress is strongly influenced by two key attributes; one is trap distribution and another is network architecture. Apparently, the variation of trap distribution may be not a crucial factor in exploring the nature of transfer channel, because the indispensable electron reservoir is still steadily embedded in all the $Zn_{1-x}Ca_xGa_2O_4$ solid-solutions (Fig. 4c). To probe the evolution of topological network-dependent

topochemical coordination, the systematic characterization, such as, XRD, solid NMR, EDX mapping and Raman spectra should be conducted[32]. XRD peaks in $Z_{1-x}C_xGO$ (x = 0.1, 0.4, 0.5 and 0.7) samples indicate their $ZnGa_2O_4$ spinel solid-solution nature, while the superimposed peaks in samples $Z_{0.5}C_{0.5}GO$ and $Z_{0.3}C_{0.7}GO$ can be well indexed by the diffraction peaks of $ZnGa_2O_4$ and $CaGa_2O_4$ (Fig. 4d, and Supplementary Fig. S10). EDX mapping analysis reveals the solid-solutions have uniform distribution of Ca elements in all of the spinel solid-solutions (Supplementary Fig. S11, S12 and Fig. 4e). EDX experimental composition approximating the theoretical value supports the successful inclusion of Ca elements in spinel crystals (Supplementary Table S2).

^{71}Ga NMR spectra have provided some insights into the coordination variation of Ga center in $ZnGa_2O_4$ and $CaGa_2O_4$ phosphors, due to the incorporation of Cr and Nd. it is also expected to manifest its ability in resolving the question of topochemical configuration's evolution process, as the addition of Ca element. As shown in Fig. 4f, with increasing Ca content (0, 0.2, 0.4 and 0.7), two resonances at 170 and 31 ppm in ^{71}Ga NMR spectra increasingly present the linear broadening. In these solid solutions, Zn-O and Ga-O tetrahedron could suppress the intrusion of Ca element due to the mismatch of coordination configuration. In fact, to steady Ca ion, parts of Ga-O octahedron must reorient to form the new polyhedron network Ca-O octahedron along with the transformation from Ga-O octahedron to Ga-O tetrahedron due to the decrease of Zn-O tetrahedron. In detail, for the samples $Z_{1-x}C_xGO$ (x = 0, 0.2 ,0.4), the motion of local hybrid coordination-networks evolution include: (1) the precipitation of Ca on the lattice site of octahedron Ga, giving rise to the broadening of NMR resonance at 164 ppm; (2) the conversion from Ga-O octahedron to Ga-O tetrahedron, resulting in the enhancement of NMR resonance at 65 ppm. This interesting redeployment of network configuration thus permits the modification of topochemical state of dopants, as well as opens the possibility of bridging cascaded channels to transfer the persistent energy. To further validate the research idea aiming at the network configuration, Raman spectra of the fabricated samples also can be selected as the pertinent tool to further analyze the evolution of network architecture (Fig. 4g and Supplementary Fig. S13)[33]. In stark contrast to samples ZGO-0.5Nd and ZGO-5Nd, normalized Raman spectra of samples CGO-0.5Nd and CGO-5Nd do not exhibit the notable Raman peak shift and variation of Raman peak intensity, indicating a strong constraint of topological network to the migration of Nd ions in $CaGa_2O_4$. In fact, only two distinct Raman bands at ~1358 and 1434 cm^{-1} are present in the Raman spectrum of CGO-0.5Nd, while the Raman spectrum of ZGO-0.5Nd includes three identifiable Raman peaks at ~1341, 1389 and 1425 cm^{-1}. Thus, Raman spectra of $Z_{1-x}C_xGO$ (x = 0.1, 0.4 and 0.7) solid-solutions consequentially show a unit number decrease of Raman peaks with the increment of Ca content (inset of Fig. 4g). The variation of middle peak at 1401 cm^{-1} as a function of Ca doping content ensures the strong signature of the hybrid network structure, which is in accordance with the XRD and solid-state NMR data.

In summary, we report a principle of bridging cascaded energy transfer channels to activate long persistent phosphorescence in the second biological window and fabrication of novel near-infrared phosphorescent phosphor Cr/Nd codoped $Zn_{1-x}Ca_xGa_2O_4$ solid-solutions. Structural studies offer the powerfully fundamental evidences to explain the closed energy transfer channel from Cr^{3+} to Nd^{3+} in $ZnGa_2O_4$ phosphor and invalidation of electronic reservoir in $CaGa_2O_4$ phosphor. We believe that the ingenious solid-solution technology featuring the superiority of engineering a hybrid coordination-network opens new paths for advanced dynamic management of activation energy and gives the inspiration to design future new-wavelength, NIR phosphorescent phosphors by energy transfer.

Methods

Materials. 4N pure $CaCO_3$, Ga_2O_3, ZnO, Nd_2O_3 and Cr_2O_3 were selected as the raw materials.

Preparation of $ZnGa_2O_4$: xCr/yNd. Phosphors with molar compositions of $ZnGa_2O_4$: xCr/yNd (x = 0, 0.5%, 5%, 10%, 20%; y = 0, 0.5%, 5%, 10%, 20%), (Supplementary Table S1) were prepared by the solid state reaction method. The reaction included a two-step thermal treatment (i.e., initial calcination at 800 °C for 5 h, secondary calcination at 1350 °C for 3 h).

Preparation of $CaGa_2O_4$: xCr/yNd. Phosphors with molar compositions of $CaGa_2O_4$: xCr/yNd (x = 0, 0.5%; y = 0, 0.5%, 5%, 10%), (Supplementary Table S1) were prepared by the solid state reaction method. The reaction included a two-step thermal treatment (i.e., initial calcination at 800 °C for 5 h, secondary calcination at 1200 °C for 3 h).

Preparation of $Zn_{1-x}Ca_xGa_2O_4$: 0.5Cr/yNd. Phosphors with molar compositions of $Zn_{1-x}Ca_xGa_2O_4$: 0.5Cr/yNd (y = 0, 0.5%, 1%, 2%; x = 0.1, 0.2, 0.3, 0.4, 0.5, 0.7), (Supplementary Table S1) were prepared by the solid state reaction method. The reaction included a two-step thermal treatment (i.e., initial calcination at 800 °C for 5 h, secondary calcination at 1350, 1350, 1300, 1300, 1270, 1250 °C for 3 h as a function of x, respectively).

Characterization. The prepared materials were analyzed by X-ray diffraction (Cu/Kα) to confirm the sole crystalline phase. Room-temperature photoluminescence (PL), photoluminescence excitation (PLE) spectra, afterglow spectra and decay curves were measured with a high-resolution spectrofluorometer (UK, Edinburgh Instruments, FLS920) equipped with a 500 W Xenon lamp as an excitation source, with a Hamamatsu R928P visible photomultiplier (PMT) (250–850 nm) and a liquid nitrogen-cooled Hamamatsu R5509-72 NIR PMT as the detectors. TL glow curves and TL excitation (TLE) spectra were measured with a FJ-427A TL meter (China, Beijing) to characterize defect properties. Unless otherwise mentioned, the samples were pre-annealed at 600 K before testing, and some measurements were taken after pre-irradiating the samples for 10 min by using a xenon lamp. EDX images are characterized by a field emission scanning electron microscopy (FE-SEM), Nova NanoSEM 430. ^{71}Ga Hahn echo NMR experiments were performed on Bruker Avance III spectrometers operating at magnetic fields of 111.4 T corresponding to ^{71}Ga Larmor frequencies of 152.54 MHz) using Bruker 2.5 mm triple and double resonance probe heads. The 90^0 degree pulse length is 1.25 μm with a recycle delay of 8s. ^{71}Ga chemical

shifts were referenced relative to a 1.0 M aqueous solution of $Ga(NO_3)_3$. All ^{71}Ga spectra were fitted using the Dmfit software. Raman spectra were collected with a Renishaw inVia Raman microscope irradiated by a visible laser at 532 nm.

References

1. Maldiney, T. *et al.* The *in vivo* activation of persistent nanophosphors for optical imaging of vascularization, tumours and grafted cells. *Nat. Mater.* **13,** 418–426 (2014).
2. Abdukayum, A., Chen, J. T., Zhao, Q. & Yan, X. P. Functional near infrared-emitting Cr^{3+}/Pr^{3+} co-doped zinc gallogermanate persistent luminescent nanoparticles with superlong afterglow for *in vivo* targeted bioimaging. *J. Am. Chem. Soc.* **135,** 14125–14133 (2013).
3. Pan, Z. W., Lu, Y. Y. & Liu, F. Sunlight-activated long-persistent luminescence in the near-infrared from Cr^{3+}-doped zinc gallogermanates. *Nat. Mater.* **11,** 58–63 (2012).
4. Maldiney, T. *et al.* Gadolinium-doped persistent nanophosphors as versatile tool for multimodal *in vivo* imaging. *Adv. Funct. Mater.* **25,** 331–338 (2015).
5. Hong, G. S. *et al.* Through-skull fluorescence imaging of the brain in a new near-infrared window. *Nat. Photonics.* **8,** 723–730 (2014).
6. Lv, R. C. *et al.* A yolk-like multifunctional platform for multimodal imaging and synergistic therapy triggered by a single near-infrared light. *Acs Nano*. **9,** 1630–1647 (2015).
7. Hong, G. S. *et al. In Vivo* Fluorescence Imaging with Ag_2S Quantum Dots in the Second Near-Infrared Region. *Angew. Chem. Int. Edit.* **51,** 9818–9821 (2012).
8. Li, Y. *et al.* Tailoring of the trap distribution and crystal field in Cr^{3+}-doped non-gallate phosphors with near-infrared long-persistence phosphorescence. *NPG. Asia. Mater.* **7,** e180(1)-(11) (2015).
9. Horike, S., Umeyama, D., Inukai, M., Itakura, T. & Kitagawa, S. Coordination-network-based ionic plastic crystal for anhydrous proton conductivity. *J. Am. Chem. Soc.* **134,** 7612–7615 (2012).
10. Oh, M. & Mirkin, C. A. Chemically tailorable colloidal particles from infinite coordination polymers. *Nature.* **438,** 651–654 (2005).
11. Desiraju, G. R. Cryptic crystallography. *Nat. Mater.* **1,** 77–79 (2002).
12. Zaworotko, M. J. Crystal engineering comes of age. *Nat. Chem.* **3,** 653–653 (2011).
13. Miyakawa, T. & Dexter, D. Phonon sidebands, multiphonon relaxation of excited states, and phonon-assisted energy transfer between ions in solids. *Phys. Rev. B* **1,** 2961–2969 (1970).
14. Takasaki, H., Tanabe, S. & Hanada, T. Long-lasting afterglow characteristics of Eu, Dy codoped SrO-Al_2O_3 phosphor. *J. Ceram. Soc. Jpn.* **104,** 322–326 (1996).
15. Zhou, S. F., Jiang, N., Wu, B. T., Hao, J. H. & Qiu, J. R. Ligand-driven wavelength-tunable and ultra-broadband infrared luminescence in single-ion-doped transparent hybrid materials. *Adv. Funct. Mater.* **19,** 2081–2088 (2009).
16. Yan, S. *et al.* Zinc gallogermanate solid solution: A novel photocatalyst for efficiently converting CO_2 into solar fuels. *Adv. Funct. Mater.* **23,** 1839–1845 (2013).
17. Kobayashi, G. *et al.* Isolation of solid solution ohases in size-controlled Li_xFePO_4 at room temperature. *Adv. Funct. Mater.* **19,** 395–403 (2009).
18. Tsuji, I., Kato, H., Kobayashi, H. & Kudo, A. Photocatalytic H_2 evolution reaction from aqueous solutions over band structure-controlled $(AgIn)_xZn_{2(1-x)}S_2$ solid solution photocatalysts with visible-light response and their surface nanostructures. *J. Am. Chem. Soc.* **126,** 13406–13413 (2004).
19. Arico, A. S., Bruce, P., Scrosati, B., Tarascon, J. M. & Van Schalkwijk, W. Nanostructured materials for advanced energy conversion and storage devices. *Nat. Mater.* **4,** 366–377 (2005).
20. Bessière, A. *et al.* Storage of visible light for long-lasting phosphorescence in chromium-doped zinc gallate. *Chem. Mater.* **26,** 1365–1373 (2014).
21. Yraola, E., Molina, P., Plaza, J. L., Ramírez, M. O. & Bausá, L. E. Spontaneous emission and nonlinear response enhancement by silver nanoparticles in a Nd^{3+}-doped periodically poled $LiNbO_3$ laser crystal. *Adv. Mater.* **25,** 910–915 (2013).
22. Li, Y. *et al.* A strategy for developing near infrared long-persistent phosphors: taking $MAlO_3$: Mn^{4+}, Ge^{4+} (M=La, Gd) as an example. *J. Mater. Chem. C* **2,** 2019–2027 (2014).
23. Li, Y. *et al.* Long persistent and photo-stimulated luminescence in Cr^{3+}-doped Zn–Ga–Sn–O phosphors for deep and reproducible tissue imaging. *J. Mater. Chem. C* **2,** 2657–2663 (2014).
24. Ren, J. J. & Eckert, H. A Homonuclear Rotational Echo Double-Resonance Method for Measuring Site-Resolved Distance Distributions in I=1/2 Spin Pairs, Clusters, and Multispin Systems. *Angew. Chem. Int. Edit.* **51,** 12888–12891 (2012).
25. Barry, B. M. & Gillan, E. G. Low-temperature solvothermal synthesis of phosphorus-rich transition-metal phosphides. *Chem. Mater.* **20,** 2618–2620 (2008).
26. Allix, M. *et al.* Considerable improvement of long-persistent luminescence in germanium and tin substituted $ZnGa_2O_4$. *Chem. Mater.* **25,** 1600–1606 (2013).
27. Trojan-Piegza, J., Niittykoski, J., Holsa, J. & Zych, E. Thermoluminescence and kinetics of persistent luminescence of vacuum-sintered Tb^{3+}-doped and Tb^{3+}, Ca^{2+}-codoped Lu_2O_3 materials. *Chem. Mater.* **20,** 2252–2261 (2008).
28. Dehnicke, K. & Greiner, A. Unusual complex chemistry of rare-earth elements: Large ionic radii-small coordination numbers. *Angew. Chem. Int. Edit.* **42,** 1340–1354 (2003).
29. RepSaines, P. J., Elcombe, M. M. & Kennedy, B. J. Lanthanide distribution in some doped alkaline earth aluminates and gallates. *J. Solid. State. Chem.* **179,** 613–622 (2006).
30. Zhuang, Y., Ueda, J. & Tanabe, S. Tunable trap depth in $Zn(Ga_{1-x}Al_x)_2O_4$: Cr, Bi red persistent phosphors: considerations of high-temperature persistent luminescence and photostimulated persistent luminescence. *J. Mater. Chem. C* **1,** 7849–7855 (2013).
31. Li, Y. *et al.* Anti-stokes fluorescent probe with incoherent excitation. *Sci. Rep.* **4,** 1–6 (2014).
32. Krumpel, A. H., Bos, A. J. J., Bessière, A., van der Kolk, E. & Dorenbos, P. Controlled electron and hole trapping in YPO_4:Ce^{3+}, Ln^{3+} and $LuPO_4$:Ce^{3+}, Ln^{3+} (Ln=Sm, Dy, Ho, Er, Tm). *Phys. Rev. B* **80,** 085103 (1)-085103(10) (2009).
33. Van, den. Eeckhout., K., Poelmanm, D. & Smet, P. Persistent luminescence in Non-Eu^{2+}-doped compounds. A Review. *Materials.* **6,** 2789–2818 (2013).

Acknowledgements

This work was financially supported by National Natural Science Foundation of China (Grant Nos 51132004, 51072754, 51472091, 61475174), Guangdong Natural Science Foundation (Grant Nos S2011030001349, 2014A030310444), National Basic Research Program of China (Grant Nos 2011CB808100), China Postdoctoral Science Foundation (Grant Nos 2015M570707), 100 Talents Program of Chinese Academy of Sciences and Fundamental Research Funds for the Central Universities (Grant Nos 2013ZM0001, 2015ZM089). This work was also supported by the Open Fund of the State Key Laboratory of High Field Laser Physics (Shanghai Institute of Optics and Fine Mechanics.).

Author Contributions

J.R.Q. conceived and designed the experiments, and was responsible for the project planning. X.X.Q. prepared the samples. X.X.Q., Y.L. and Y.L.W. investigated the spectroscopic properties. J.J.R. and R.L.Z. carried out the NMR study. Y.L. wrote the manuscript. J.R.Q., M.G., S.F.Z., Z.J.M., K.F. and G.P.D. checked the manuscript. All authors were involved in the discussion of the experimental results.

Additional Information

Supplementary information accompanies this paper at http://www.nature.com/srep

Competing financial interests: The authors declare no competing financial interests.

How to cite this article: Qin, X. *et al.* Hybrid coordination-network-engineering for bridging cascaded channels to activate long persistent phosphorescence in the second biological window. *Sci. Rep.* **6**, 20275; doi: 10.1038/srep20275 (2016).